Performance of systematic fully grouted rockbolts and shotcreted layer in circular tunnel under the hydrostatic conditions using 3D finite difference approach

Performance of systematic fully grouted rockbolts and shotcreted layer in circular tunnel under the hydrostatic conditions using 3D finite difference approach

Milad Zaheri [a], Masoud Ranjbarnia [b]*, Pierpaolo Oreste [c]

[a] *Department of geotechnical Engineering, Faculty of civil engineering, University of Tabriz, 29 Bahman Blvd, Tabriz, Iran, Miladzaheri@tabrizu.ac.ir*

[b] *Department of geotechnical Engineering, Faculty of civil engineering, University of Tabriz, 29 Bahman Blvd, Tabriz, Iran, M.ranjbarnia@tabrizu.ac.ir*

[c] *Department of Environmental, Land and Infrastructure Engineering, Politecnico di Torino, Corso Duca degli Abruzzi, Torino 24-10129, Italy, Pierpaolo.oreste@polito.it*

Performance of systematic fully grouted rockbolts and shotcreted layer in circular tunnel under the hydrostatic conditions using 3D finite difference approach

Fully grouted rockbolts with or without shotcrete layer are widely used in practice. Thus, studying their roles in decreasing induced tunnel strains is an important issue. In 2D analytical methods, a unit length of the tunnel along its longitudinal axis is considered. Therefore, the influence radius of a bolt, as well as the non-uniform strains in the longitudinal axis cannot be highlighted. FLAC^{3D} software was used to determine these parameters. After verifying the conducted finite difference program, a parametric study was performed to study the rockbolts and the shotcrete layer roles on controlling the induced tunnel strains. The results indicate that in the very severe squeezing rock mass conditions, the ratio of the strains in the middle between two bolts to that of in the rockbolt head is slightly high. Also, the influence radius of a bolt is almost the same for the cases conducted in this research.

Keywords: Deep tunnels; Numerical simulation; Rockbolts; Shotcrete

Introduction

Due to effectiveness, efficiency, minimum installation space, and cost, grouted rockbolts are frequently used as a favorable support system in underground mining and tunneling operation. In addition, the possibility to be combined with the other support systems such as the shotcrete layer to constitute a hybrid system is the other benefit of grouted bolts usage.

Regarding the performance of only grouted rockbolts in tunnel stabilization, numerous studies have been carried out by analytical and numerical approaches. The presented analytical methods can be included in either of two following groups:

- the reinforced medium around the tunnel is considered as an equivalent composite material i.e. its mechanical properties includes both the rock and the

rockbolt (Indraratna and Kaiser 1990a, 1190b, Grasso et al. 1989, Fahimifar and Ranjbarnia 2009, Osgoui and Oreste 2007, 2010, Ranjbarnia et al. 2016);

- the contribution of the bolt to the rock around tunnel is in the form of a uniform radial compressive stress which is applied to the rock within the influence domain of each bolt (Stille et al. 1989, Oreste and Peila 1996, Li and Stillborg 1999, Cai et al. 2004, Oreste 2004, 2008a, b 2009, 2013, Fahimifar and Soroush 2005, Guan et al. 2007, Tan et al. 2008, Carranza-Torres 2009, Fahimifar and Ranjbarnia 2009, Bobet and Einstein 2011, Ranjbarnia et al. 2014, 2015).

From these two approaches, it turns out the uniform radial stress around tunnel and so forth the uniform deformation of the tunnel wall between bolts. If the spacing between the bolts is much smaller than the tunnel radius and the bolt length, it is an unexpected approximation. However, if the tunnel is located in a very squeezing condition (a deep tunnel in a weak rock), a compliant rock deforms unevenly between bolts. The non-uniform deformations of the rock material around the rockbolt may induce large bending moments on the shotcrete layer (if exist).

Ranjbarnia et al. (2016) found that the distribution of the induced radial stress in the medium around a bolt is exponential, which is maximum in the vicinity of the bolt and dwindles at far distances from the bolt. Accordingly, the shear stress propagation from the bolt-rock interface toward location between the bolts (in the tangential direction of the tunnel section) was obtained. However, one of the limitations is two-dimensional modeling of the analytical method which does not consider the bolt spacing in the longitudinal direction.

In the previous numerical studies, on the other hand, investigation of some other complex issues have been the aim e.g. non-uniform distribution of bolts around a tunnel in the non-hydrostatic in-situ stress (Bobet and Einstein 2011), analyses of a reinforced

non-circular tunnel (Zhang et al. 2015), the presence of systematic discontinuities in the reinforced rock mass (Nie et al. 2014, 2018), evaluation of dynamic loading on the reinforced tunnels (Mortazavi and Alavi 2013, Tahmasebinia et al. 2018), consideration of crack in the grout between the rockbolt and the medium i.e. say de-bonding in the rock bolt-medium interface (Nemcik et al. 2014, Zhu et al. 2015, Chang et al. 2017). However, neither the issue of non-uniform deformation of the rock between the bolts nor the stresses distribution has been addressed.

Therefore, by the numerical modelling with FLAC^{3D}, parametric analyses are conducted to find the strains and stresses in the location between grouted bolts which are systematically installed over infinite length of a circular tunnel. The "radius of influence" of any grouted bolt is obtained for different conditions of the tunnel depth and the rock mass quality. Then, the induced bending moment on the shotcrete layer is calculated to see in what circumstance it can be ignored.

Three dimensional numerical modeling Procedures

A parametric study was conducted by the finite difference program FLAC^{3D} to observe in detail how fully grouted rockbolts control the tunnel wall displacements. The adopted numerical running procedures consisted of the following four steps:

1) Setting up a model including geometry, boundary conditions, and initial stresses; then solving the problem to obtain initial equilibrium condition;
2) Excavation or advancement of the tunnel face to a specific length;
3) Spray of a shotcrete layer (if any) in the new excavated length and installation of fully grouted rockbolts (the new excavated length will equal to the longitudinal distance between the bolts); and

4) Repeat of the above steps 2 and 3 until the tunnel face reaches the distance of three tunnel diameter from an assumed reference section.

The first critical issue after model construction is to determine the location of the model boundaries as well as the mesh sizes so their unsatisfactory effects on results are diminished. For this reason, each dimension of the model was selected as $10D_t$ (where D_t is the tunnel diameter). The elements size was gradually increased in the radial direction from the tunnel center towards the outer boundary (Figure 1). Before, coarseness of the meshes was also analyzed. In Y direction (the longitudinal direction of the tunnel), the mesh sizes were refined around the reference section (e.g. at Y = 21 m in which the excavation length equals to 1 m) where strains and displacements of the tunnel were to be studied in detail. As a result, the constructed model was divided from 64640 to 193280 hexagonal elements considering the number of bolts.

[Figure 1 near here]

A lithostatic pressure (P_0) was exerted to all of the artificial boundaries (i.e. the horizontal to vertical in-situ stresses ratio was $K_0 = 1$), and the variation of the vertical and the horizontal in-situ stresses values with the depth was neglected (Figure 2). Although the horizontal stress is always greater than the vertical stress in deep excavations, one of the main purposes of the paper is to obtain the domain influence of bolts in different quality of rock masses and tunnel depths (the results were given in terms of $\frac{\sigma_{cm}}{P_0}$). Therefore, it is well possible to find it only in the hydrostatic in-situ stress condition. In fact, the simplest case of in-situ stress should be considered in models rather than non-hydrostatic condition. That is, if the non-hydrostatic in-situ stress was considered in the simulations, the displacements of tunnel wall in different positions considerably would be influenced by horizontal stress value. In these cases, it is impossible to draw a conclusion on the domain influence of a bolt. Because, in each

position of the tunnel wall, a different value will be obtained for the domain influence of a bolt. Furthermore, the domain influence of a bolt is inherently depended upon to tunnel depth and rock mass quality. Then, the hydrostatic in-situ stress was considered in this paper. After this step, the problem was left in running until the equilibrium state was reached and then, the velocities and the displacements in the whole of the model were set to zero.

[Figure 2 near here]

A circular tunnel with the radius (R_t) of 5 m was excavated in an isotropic and a homogeneous rock mass (the problem is under axis-symmetric condition, then modelling only one-quarter of the real model is possible). The excavation was continued until the tunnel face reached to the next section of the bolts placement. Noting that the length of tunnel advance was equal to the distance between adjacent bolts in the longitudinal direction of the tunnel. A shotcrete layer was sprayed (if any) and then all bolts were systematically installed in the circumferential direction (Figures. 3 and 4).

[Figure 3 near here]

[Figure 4 near here]

To simulate the shotcrete layer and the fully grouted rockbolts, the Liner and the Cable elements embedded in the FLAC^{3D} software were respectively used. The Liner elements which have a linear-elastic behavior are used to model thin liners for which both shear-directed frictional interaction and normal-directed tensile/compressive interaction with the host medium occur (Itasca 2007).

By knowing the bulk modulus (K_r) and the shear modulus (G_r) of the rock mass, and finding the smallest dimension of a neighboring zone in the normal direction of the shotcrete layer (Δz_{min}), both of the normal and the shear stiffnesses of the interface

between the shotcrete layer and the rock mass can be found via one hundred times of equation (1) (Itasca 2007).

$$max\left[\frac{K_r + \frac{4}{3}G_r}{\Delta z_{min}}\right] \quad (1)$$

For the mono-dimensional Cable elements, knowing the bolt's diameter (d), the grout (annulus) thickness (t_g), and the shear modulus of the grout (G_g), the grout stiffness can be found via equation (2) (Itasca 2007).

$$k_g = \frac{2\,\pi G_g}{10\ln(1 + \frac{2t_g}{d})} \quad (2)$$

The Cables behave as an elastic-perfectly plastic in both the tension and the compression stresses. The interaction of these elements with the medium (here is grout or rock mass) occurs via shear springs. By neglecting the frictional component of the grout, the shear strength of the grout per unit length (c_g) is calculated by equation (3) (Itasca 2007).

$$c_g = \pi(d + 2t_g)\tau_I Q_B \quad (3)$$

where t_g is the grout thickness, Q_B represents the quality of the bond between the grout and the medium, and τ_I is one half of the minimum of the rock mass and the grout uniaxial compression strength. However, if the failure does not occur in the interface of the rock mass and the grout, it may occur between the bolt and the grout interface (Itasca 2007). In this study, a perfect bonding between the rock and the grout was foreseen. Thus, Q_B was assumed as 1.

The complex of bolt head components i.e. nut, washer, and stiff steel plate beds tightly on its basement (shotcrete or smooth seat) on the tunnel wall. That is, a perfect constraint was foreseen on the bolt head, and no relative movements occurred between the bolt and the rock mass in the vicinity of the steel plate. To simulate this

phenomenon, the cable nodes located in the tunnel perimeter were rigidly attached to the adjacent zone.

The step by step tunnel excavation and installation of the supporting system (s) were performed by FISH programming language embedded within FLAC^{3D} software.

The bolts length (L_b) were chosen as a value to be greater than the plastic zone around the tunnel. For this purpose, try and error procedures were carried out starting from the unsupported tunnel plastic thickness.

The rock mass was assumed to obey the Mohr-Coulomb failure criterion. Using equations (4) and (5), the equivalent friction angle and cohesion from the nonlinear Hoek-Brown failure criterion respectively can be obtained by Hoek et al. (2002).

$$\emptyset' = sin^{-1}[\frac{6am_b(s + m_b\sigma'_{3n})^{a-1}}{2(1+a)(2+a) + 6am_b(s + m_b\sigma'_{3n})^{a-1}}] \quad (4)$$

$$c' = \frac{\sigma_{ci}[(1+2a)s + (1-a)m_b\sigma'_{3n}](s + m_b\sigma'_{3n})^{a-1}}{(1+a)(2+a)\sqrt{1 + \frac{6am_b(s + m_b\sigma'_{3n})^{a-1}}{(1+a)(2+a)}}} \quad (5)$$

where σ_{ci} is the uniaxial compression strength of intact rock and σ'_{3n} can be found by equation (6). As well, parameters s, m_b and a can be calculated from equations (7) - (9) (Hoek et al. 2002).

$$\sigma'_{3n} = \frac{\sigma'_{3max}}{\sigma_{ci}} \quad (6)$$

$$s = e^{\frac{GSI-100}{9-3D}} \quad (7)$$

$$m_b = m_i e^{\frac{GSI-100}{28-14D}} \quad (8)$$

$$a = 0.5 + \frac{1}{6}\left(e^{-\frac{GSI}{15}} - e^{-\frac{20}{3}}\right) \quad (9)$$

where GSI is geological strength index of the rock mass, m_i and σ_{ci} are the constant parameter and the uniaxial strength of the intact rock, respectively; and D is the

disturbance degree of the rock mass. D parameter here assumed as zero. This assumption is reasonable in an excellent quality controlled blasting, mechanical or hand excavation in poor quality rock masses (no blasting) due to minimal disturbance of the surrounding rock mass of a tunnel (Hoek et al. 2002). If the other values are assumed for D, the values of m_b, s, a will vary. However, this assumption does not alter the purpose of the paper. The uniaxial compressive strength of the rock mass (σ_{cm}) is

$$\sigma_{cm} = s^a \sigma_{ci} \tag{10}$$

For tunnels, the relation $\sigma'_{3\max}$ is calculated by Hoek et al. (2002):

$$\sigma'_{3max} = 0.47\sigma'_{cm}\left(\frac{\sigma'_{cm}}{\gamma_r H}\right)^{-0.94} \tag{11}$$

$$\sigma'_{cm} = \sigma_{ci}.\frac{(m_b + 4s - a(m_b - 8s))(\frac{m_b}{4} + s)^{a-1}}{2(1+a)(2+a)} \tag{12}$$

where γ_r and H respectively are the unit weight of rock mass and the tunnel depth.

The rock mass elasticity modulus can be found by Hoek et al. (2006):

$$E\ (MPa) = 100000\left(\frac{1-\frac{D}{2}}{1+e^{\frac{75+25D-GSI}{11}}}\right) \tag{13}$$

Depending on GSI value, three different stress – strain laws can be expected for the rock masses (Hoek and Brown 1997):

- For rock masses which have low values of GSI (smaller than about 25), the rock masses have an elastic perfectly plastic behavior, and the dilation angle is zero. Therefore, the rock mass strength parameters (such as the equivalent friction angle and the cohesion and so on) remain constant after the elastic limit;
- For rock mass with GSI values between 25 and 75, the dominant behavior is strain softening. In this case, the residual value of GSI can be estimated from Table 1 (Alejano et al. 2010), and the other associated parameters can be

obtained by equations (4) and (5) (by using Roclab software (Rocscience 2007) or by using FISH programming language embedded within FLAC^{3D} software). The average dilation angle is $\frac{\emptyset}{8}$. The softening parameters which reflect the extent of the plastic softening strain in the stress-strain curve before the residual stage are function of GSI and the tunnel depth, and can be calculated by an approach presented by Alejano et al. 2010.

- For the values of GSI greater than about 75, an elastic-brittle plastic behavior was assigned to the rock mass while the dilation angle is about $\frac{\emptyset}{4}$.

[Table 1 near here]

Table 2 presents the value of the parameters which were constant in parametric studies.

[Table 2 near here]

Verification and calibration

To verify the predictions of the tunnel convergence by the 3D numerical simulation, the reported actual performance of bolts (or combination of bolts and the shotcrete layer) in the Kielder experimental tunnel was selected. This tunnel with radius 1.65 m subjected to the in-situ stress 2.56 MPa was highly unstable in the mudstone (with geo-mechanical properties reported in Table 3) and required the most efficient support. One of the sections in this rock mass was only supported by grouted rockbolts while the shotcrete layer was added to the rockbolts in two other sections (with properties reported in Table 3) (Ward et al. 1976 and 1983, Freeman 1978).

[Table 3 near here]

In the numerical model, the shotcrete layer (if any) was placed from the last shotcreted location to the excavation face i.e. in the length of 0.9 meters while the bolts were installed just in front of the face. Assigning the elastic perfectly-plastic constitutive model to the rock mass, and performing sensitive analyses to the boundary location and the mesh sizes, the average tunnel displacement after full advancement of the tunnel face from the reference point was 2.5 mm and 3.46 mm in the shotcreted sections and the bolted section, respectively, which were found to be in close agreement with measured data. Because, according to Ward et al. (1976, 1983), total short-term movement of the tunnel wall in these sections was respectively 2-3 mm and 4-5 mm.

Note that the bond strength had no significant effects on the obtained results provided it is not so small that de-bonding occurred between the bolt and the medium.

To evaluate the predictions of the numerical model for the induced stresses due to the bolting effect, its results are compared with those of an analytical solution. Ranjbarnia et al. (2016) proposed that the increase of the radial stress of medium by the bolting effect ($\Delta\sigma_r$) can be calculated by

$$\Delta\sigma_r = aexp(-br') \tag{14}$$

where r' is the perpendicular distance from the bolt perimeter surface (along the axis), and the parameters a and b can be found by the boundary conditions as follow

- at $R = \mp\infty \rightarrow \Delta\sigma_r = 0$

where R is the influence radius of a rockbolt. For practical purposes, R is considered as a distance where $\Delta\sigma_r$ =1% of the maximum value (i.e. a). Solving equation (14) leads $bR = 4.60$. The a parameter can be calculated by the fact that the

average increase of the radial stress due to the bolting effect (i.e. $\Delta\sigma_r = \frac{T}{S_c S_l}$, where T is the bolt load; and S_l and S_c are the spacing between bolts in the longitudinal and circumferential direction, respectively) is equal to the average value by equation (14).

If the parameter R in Eq. (14) is assumed to be identical to the value given by the numerical modeling, the predicted increase of the radial stress in the tunnel wall by the analytical and numerical models for the case of Kielder Tunnel are depicted in Figure 5, which shows a good agreement.

[Figure 5 near here]

The parametric study and the input data

Hoek and Marinos (2000) presented a classification by which the ratio of the uniaxial compression strength of the rock mass to the in-situ stress (σ_{cm}/P_0) indicates the tunnel squeezing potential problem. Regarding to this research, for each of the squeezing group, the adequate supporting systems were recommended. If the tunnel strain is less than 2.5%, the shotcrete layer together with the rockbolts can be utilized, however, this recommendation is not considered here. In other words, fully grouted rockbolts (with or without the shotcrete layer) were considered for all the cases.

In this paper, depending on σ_{cm}/P_0 value, three classes can be considered (see Table 4). Based on this classification, numerous analyses were performed in which several values of GSI were accompanied with several conventional tunnel depths (i.e. 200, 500 and 800 m), and a value of σ_{ci} was assigned to them so that for each value of $\frac{\sigma_{cm}}{P_0}$, at least three various rock masses were considered (σ_{cm} is function of GSI and σ_{ci}) (Table 5).

[Table 4 near here]

[Table 5 near here]

As depicted in Figure 6, the tunnel displacement in the bolt head and in the middle between two rockbolts are respectively indicated by Δ_b and Δ_m, and the corresponding strains by ε_b and ε_m.

All of the analyses were performed in the absence and the presence of bolts to obtain the tunnel convergence. For each case of analyses, a minimal space for adjacent bolts (as a bolting pattern) was assumed and then, it was gradually increased so that the tunnel convergence between the bolts became so great that it finally equaled to that of the unsupported tunnel (i.e. $\Delta_m = \Delta_{un}$ in Figure 6).

[Figure 6 near here]

Results and discussion

The displacements of tunnel wall between the bolts and influence domain of each bolt

In this section, grouted rockbolts role was particularly addressed in detail on the confinement of the tunnel convergence. Figure 7 depicts an example of the non-uniform displacements of the tunnel wall where due to less contribution between two bolts, the displacement is greater. At the tangential direction, it is a little bit smaller than that of the longitudinal direction because of smaller bolts spacing i.e. 0.98 m in comparison with 1 m. Hereafter, only the results of the longitudinal direction are discussed.

[Figure 7 near here]

Figure 8 shows convergence (or strain ε_m (%)) of the reinforced tunnel between two bolts against different values of bolts spacing for various classes of $\frac{\sigma_{cm}}{P_0}$. For comparison, the convergence of the unsupported tunnel is also shown by a dash line. As

seen, when $\frac{\sigma_{cm}}{P_0}$ ratio is less than 0.1, the strains magnitude, as well as strains difference of the unsupported and the supported tunnels for lower bolt spacing are considerable.

[Figure 8 near here]

Comparison of the unsupported and the supported tunnel results shows that rockbolts in the class C have a major influence on the controlling of strains, and the strain can be reduced about 12% (Figure 8c). It should be noted that the strain values in the rock mass with $\frac{\sigma_{cm}}{P_0}$ greater than and equal to 0.25 are low and the rockbolt influence can be neglected (Figure 8a). However, in these conditions, the use of the rockbolts is not allowable and other supporting systems are recommended (see Hoek and Marinos 2000).

A notable point in Table 6 is that although σ_{ci} value in test 2 is greater than that of in test 3, the rock mass with lower GSI has notably higher tunnel strain than the rock mass with greater GSI value (the lithostatic pressures and $\frac{\sigma_{cm}}{P_0}$ ratio are constant for these tests). It means that the rock mass with the perfectly plastic behavior intensifies this difference. The GSI value can play several roles in the elastic modulus of the rock mass (see equation (13)), the shear strength components (such as the friction angle and the cohesion) and also the material stress – strain patterns.

By analyzing this table, it can be concluded that by multiplying 1.02 (an average value) and the strain (or the displacement) induced in the bolt location, the strain (or the displacement) in the middle of bolts can be obtained. As well, the amount of the non-uniformity of the strains has an inverse trend with the $\frac{\sigma_{cm}}{P_0}$ value. In other words, Δ_{rel} and ε_{rel} values decrease when the rock mass has greater $\frac{\sigma_{cm}}{P_0}$ value.

[Table 6 near here]

The above-discussed displacements are marked by A (the circumferential direction) and B (the longitudinal direction) in Figure 9. As expected, an extreme case of the maximum strain (ε_{mbf}), that cannot be recorded in the 2D simulations, can be occurred in the middle of four bolts (i.e. the point C).

[Figure 9 near here]

In this table, the $\frac{\varepsilon_{mbf}}{\varepsilon_b}$ ratios for the cases in which the longitudinal distance between the bolts are equal to 1 m are also presented. As expected, the values of $\frac{\varepsilon_{mbf}}{\varepsilon_b}$ are slightly greater than $\frac{\varepsilon_m}{\varepsilon_b}$. If this distance is increased, $\frac{\varepsilon_{mbf}}{\varepsilon_b}$ ratio can also increase. However, in the design of bolts for a tunnel, it is recommended that rockbolt spacing is chosen small.

The bolting space in which the strains of the supported tunnel is almost equaled to that of the unsupported tunnel is named as the influence radius of a bolt (see section 3). According to Table 7, it can be concluded that the influence radius of a bolt (an average value) is greater in a tunnel with lower burial depth. Also, this parameter has an inverse relation with the GSI value. In other words, the greater the GSI value, the lower the influence radius of a bolt. As well, in sections of a tunnel in which the intact rock has an adequate uniaxial compression strength comparing to the other sections, the longitudinal distance between the bolts can be selected higher only if the other conditions (such as the tunnel depth and the GSI value) remain the same. This procedure can effectively decrease the costs and the time of tunnel construction.

[Table 7 near here]

Tunnel supported by grouted rockbolts and shotcrete layer

It is clear that due to the addition of the shotcrete layer to bolts, the tunnel undergoes less strains (compare Tables 6 and 8). The extent of this strain reduction depends upon the shotcrete properties (i.e. thickness and Elasticity Modulus), upon the rock mass properties and the bolting spaces. For this purpose, the rockbolts spacing (S_l) and the shotcrete layer thickness (t) simultaneously increased.

Similar conclusions about ε_m can be drawn in this case. For the good rock masses ($\frac{\sigma_{cm}}{P_0} > 0.25$), the shotcrete layer has not significant effect on the induced strains. Vice versa, in the other cases, the existence of the shotcrete layer can efficiently reduce the displacements and strains (see Figure 10). For example, in the class C, the strain can be reduced about 73%. On the other hand, in the other classes, this value is about 50%. Comparing the results of Tables 6 and 8, it can be seen that the strain reduction in this case is significantly greater than that of in the tunnel supported by only rockbolts.

[Table 8 near here]

[Figure 10 near here]

For the design of shotcreted tunnels, the induced bending moments are to be known. However, more relative displacements between the bolts location and between the bolts impose a more bending moment to the shotcrete layer. The magnitude of the induced bending moment depends upon the bolting spaces, the rock mass properties and the shotcrete properties (thickness and Elasticity Modulus). Thus, the maximum bending moment (M_{max}) between two bolts was recorded and the average of this for each of $\frac{\sigma_{cm}}{P_0}$ ratios is depicted in Figure 11. As seen in this figure, as $\frac{\sigma_{cm}}{P_0}$ is greater than 0.25, the maximum bending moment is not great and it can be negligible. However, when $\frac{\sigma_{cm}}{P_0}$ ratio is less than 0.1, the induced bending moment is the highest and this value must be considered in the design phase of tunneling. Furthermore, rockbolts

spacing can intensify this parameter. However, in some cases, increasing the bolting space leads the moment bending to reduce (as mentioned before, this figure shows only the average values of the maximum bending moments). This reduction can be due to the shotcrete layer thickness. Therefore, in the tunnel design, the predominant factor must be analyzed.

As seen, the difference of the induced bending moment is not high when the bolting space is increased from 1 m to 1.5 m. However, this difference is considerable as the mentioned space is enhanced from 1.5 m to 2 m (especially for the case in which $\frac{\sigma_{cm}}{P_0} \leq 0.1$).

It is obvious from Table 7 that the average influence radius of a bolt is almost 0.75 m. The results show that when the distance between two adjacent bolts is enhanced from 1 m to 1.5 m, the extra bending moment in the lining is greater than the situation in which this distance is increased from 1.5 m to 2 m. For example, in the test with $\frac{\sigma_{cm}}{P_0} = 0.14$ (GSI = 50, P_0 = 20.8 MPa, , σ_{ci} = 46.63 MPa), the maximum bending moments induced in the shotcrete when the bolting space is 1, 1.5 and 2 m are 25.46, 25.6 and 44.7 kN.m, respectively. However, in some of the tests with the lowest $\frac{\sigma_{cm}}{P_0}$ value, the reverse of this phenomena is occurred e.g., for the case in which GSI = 25, P_0 = 13 MPa, σ_{ci} = 45.96 MPa, when the distance between two adjacent bolts is selected as 1, 1.5 and 2 m, the maximum bending moment is respectively 47.85, 84.51 and 112.6 kN.m. This implies that enhancing bolting space from 1 to 1.5 m leads 36.66 kN.m extra induced lining moment. On the other hand, when this parameter is enhanced from 1.5 to 2 m causes the extra induced lining moment to be equal to 28 kN.m. However, the lining thickness more or less can influence the magnitude of the induced lining moment.

[Figure 11 near here]

Conclusions

In this research, the effects of the rock bolting and the shotcrete layer are examined numerically using FLAC^{3D} program. For this purpose, after verifying the results of Kielder experimental tunnel, a parametric study was conducted to study the rockbolts and the shotcrete layer role on the controlling of the induced strains. The given results are

- In the class C ($\frac{\sigma_{cm}}{P_0} \leq 0.1$), the difference of the strains in the unsupported and in the supported tunnels with rockbolts as well as the strain magnitude in the similar conditions is considerable;
- The tunnel strain value is a function of the bolting density, $\frac{\sigma_{cm}}{P_0}$, GSI, σ_{ci} , P_0, the constitutive model and the type of the supporting systems;
- For the cases conducted in this research, the influence radius of a bolt is function of GSI, the uniaxial compression strength of the intact rock and the tunnel depth;
- The tunnel strains in the presence of the shotcrete layer are much smaller than that of in the tunnel supported by only the rockbolts;
- In the rock masses with lower $\frac{\sigma_{cm}}{P_0}$ values, the maximum bending moment in the shotcrete layer is greater. The greater bolting space can intensify the value of this parameter;
- Bolting spaces, rock mass properties and the shotcrete thickness can influence the induced bending moment;
- In the design of tunnels, the bending moment in the shotcrete should be considered only if both $\frac{\sigma_{cm}}{P_0}$ value and bolting density are low.

References

Alejano, L., *et al.* 2010. Application of the convergence-confinement method to tunnels in rock masses exhibiting Hoek–Brown strain-softening behaviour. *International Journal of Rock Mechanics and Mining Sciences*, 1(47), 150-160. doi: https://doi.org/10.1016/j.ijrmms.2009.07.008

Bobet, A. and Einstein, H. 2011. Tunnel reinforcement with rockbolts. *Tunnelling and Underground Space Technology*, 26(1), 100-123. doi:https://doi.org/10.1016/j.tust.2010.06.006.

Cai, Y., Esaki, T. and Jiang, Y. 2004. An analytical model to predict axial load in grouted rock bolt for soft rock tunnelling. *Tunnelling and Underground Space Technology*, 19(6), 607-618. doi:https://doi.org/10.1016/j.tust.2004.02.129.

Carranza-Torres, C. 2009. Analytical and numerical study of the mechanics of rockbolt reinforcement around tunnels in rock masses. *Rock mechanics and rock engineering*, 42(2), 175-228. doi:https://doi.org/10.1007/s00603-009-0178-2.

Chang, X., *et al.* 2017. Study on grout cracking and interface debonding of rockbolt grouted system. *Construction and Building Materials*, 135, 665-673. doi:https://doi.org/10.1016/j.conbuildmat.2017.01.031.

Fahimifar, A. and Ranjbarnia, M. 2009. Analytical approach for the design of active grouted rockbolts in tunnel stability based on convergence-confinement method. *Tunnelling and Underground Space Technology*, 24(4), 363-375. doi:https://doi.org/10.1016/j.tust.2008.10.005.

Fahimifar, A. and Soroush, H. 2005. A theoretical approach for analysis of the interaction between grouted rockbolts and rock masses. *Tunnelling and Underground Space Technology*, 20(4), 333-343. doi:https://doi.org/10.1016/j.tust.2004.12.005.

Freeman, T. 1978. The behaviour of fully-bonded rock bolts in the Kielder experimental tunnel. *Tunnels & Tunnelling International,* 10(5).

Grasso, P., Mahtab, A. and Pelizza, S. 1989. Riqualificazione della massa rocciosa: un criterio per la stabilizzazione delle gallerie. *Gallerie e Grandi Opere Sotterranee,* 29(38), 35-41.

Guan, Z., *et al.* 2007. Reinforcement mechanics of passive bolts in conventional tunnelling. *International Journal of Rock Mechanics and Mining Sciences,* 44(4), 625-636. doi:https://doi.org/10.1016/j.ijrmms.2006.10.003.

Hoek, E. and Brown, E. T. 1997. Practical estimates of rock mass strength. *International Journal of Rock Mechanics and Mining Sciences,* 34(8), 1165-1186. doi:https://doi.org/10.1016/S1365-1609(97)80069-X.

Hoek, E., Carranza-Torres, C. and Corkum, B. 2002. Hoek-Brown failure criterion-2002 edition. *Proceedings of NARMS-Tac,* 1, 267-273.

Hoek, E. and Diederichs, M. S. 2006. Empirical estimation of rock mass modulus. *International Journal of Rock Mechanics and Mining Sciences,* 43(2), 203-215. doi:https://doi.org/10.1016/j.ijrmms.2005.06.005.

Hoek, E. and Marinos, P. 2000. Predicting tunnel squeezing problems in weak heterogeneous rock masses. *Tunnels and tunnelling international,* 32(11), 45-51.

Indraratna, B. and Kaiser, P. 1990a. Analytical model for the design of grouted rock bolts. *International Journal for Numerical and Analytical Methods in Geomechanics,* 14(4), 227-251. doi:https://doi.org/10.1002/nag.1610140402

Indraratna, B. and Kaiser, P., Design for grouted rock bolts based on the convergence control method. ed. *International Journal of Rock Mechanics and Mining Sciences & Geomechanics Abstracts,* 1990b, 269-281. doi:https://doi.org/10.1016/0148-9062(90)90529-B.

Itasca, 2007. Fast Lagrangian analysis of continua in 3-dimension (flac3d v3.1). Itasca Consulting Group.

Li, C. and Stillborg, B. 1999. Analytical models for rock bolts. *International Journal of Rock Mechanics and Mining Sciences,* 36(8), 1013-1029. doi:https://doi.org/10.1016/S1365-1609(99)00064-7.

Mortazavi, A. and Alavi, F. T. 2013. A numerical study of the behavior of fully grouted rockbolts under dynamic loading. *Soil Dynamics and Earthquake Engineering,* 54, 66-72. doi:https://doi.org/10.1016/j.soildyn.2013.08.003.

Nemcik, J., *et al.* 2014. Numerical modelling of failure propagation in fully grouted rock bolts subjected to tensile load. *International Journal of Rock Mechanics and Mining Sciences,* 71, 293-300. doi:https://doi.org/10.1016/j.ijrmms.2014.07.007.

Nie, W., *et al.* 2018. Effects of joints on the reinforced rock units of fully-grouted rockbolts. *Tunnelling and Underground Space Technology,* 71, 15-26. doi:https://doi.org/10.1016/j.tust.2017.07.005.

Nie, W., *et al.* 2014. Numerical studies on rockbolts mechanism using 2D discontinuous deformation analysis. *Tunnelling and Underground Space Technology,* 41, 223-233. doi:https://doi.org/10.1016/j.tust.2014.01.001.

Oreste, P. 2004. Designing of radial bolting in tunnels. *Journal of Mining science,* 40(4), 384-394. doi: https://doi.org/10.1007/s10913-004-0022-8.

Oreste, P. 2008. Distinct analysis of fully grouted bolts around a circular tunnel considering the congruence of displacements between the bar and the rock. *International Journal of Rock Mechanics and Mining Sciences,* 45(7), 1052-1067. doi:https://doi.org/10.1016/j.ijrmms.2007.11.003.

Oreste, P. 2013. Face stabilization of deep tunnels using longitudinal fibreglass dowels. *International Journal of Rock Mechanics and Mining Sciences*, 58, 127-140. doi:https://doi.org/10.1016/j.ijrmms.2012.07.011.

Oreste, P. and Peila, D., Radial passive rockbolting in tunnelling design with a new convergence-confinement model. ed. *International Journal of Rock Mechanics and Mining Sciences & Geomechanics Abstracts*, 1996, 443-454. doi:https://doi.org/10.1016/0148-9062(96)00009-5.

Oreste, P. P. 2009. Face stabilisation of shallow tunnels using fibreglass dowels. *Proceedings of the Institution of Civil Engineers - Geotechnical Engineering*, 162(2), 95-109. doi:https://doi.org/10.1680/geng.2009.162.2.95.

Oreste, P. P. and Cravero, M. 2008. An analysis of the action of dowels on the stabilization of rock blocks on underground excavation walls. *Rock mechanics and rock engineering*, 41(6), 835-868. doi:https://doi.org/10.1007/s00603-008-0162-2.

Osgoui, R. R. and Oreste, P. 2007. Convergence-control approach for rock tunnels reinforced by grouted bolts, using the homogenization concept. *Geotechnical and Geological Engineering*, 25(4), 431-440. doi:https://doi.org/10.1007/s10706-007-9120-0.

Osgoui, R. R. and Oreste, P. 2010. Elasto-plastic analytical model for the design of grouted bolts in a Hoek–Brown medium. *International Journal for Numerical and Analytical Methods in Geomechanics*, 34(16), 1651-1686. doi:https://doi.org/10.1002/nag.823.

Ranjbarnia, M., Fahimifar, A. and Oreste, P. 2014. A simplified model to study the behavior of pre-tensioned fully grouted bolts around tunnels and to analyze the

more important influencing parameters. *Journal of Mining science*, 50(3), 533-548. doi:https://doi.org/10.1134/S1062739114030156.

Ranjbarnia, M., Fahimifar, A. and Oreste, P. 2015. Practical method for the design of pretensioned fully grouted rockbolts in tunnels. *International Journal of Geomechanics*, 16(1), 04015012. doi:https://doi.org/10.1061/(ASCE)GM.1943-5622.0000464.

Ranjbarnia, M., *et al.* 2016. Analytical-numerical solution for stress distribution around tunnel reinforced by radial fully grouted rockbolts. *International Journal for Numerical and Analytical Methods in Geomechanics*, 40(13), 1844-1862. doi:https://doi.org/10.1002/nag.2517.

Rocscience, I., 2007. RocLab Version 1.031—Rock mass strength analysis using the Hoek–Brown failure criterion. Online.

Stille, H., Holmberg, M. and Nord, G., Support of weak rock with grouted bolts and shotcrete. ed. *International Journal of Rock Mechanics and Mining Sciences & Geomechanics Abstracts*, 1989, 99-113. doi:https://doi.org/10.1016/0148-9062(89)90530-5.

Tahmasebinia, F., *et al.* 2018. Numerical and analytical simulation of the structural behaviour of fully grouted cable bolts under impulsive loading. *International Journal of Mining Science and Technology*, 28(5), 807-811. doi:https://doi.org/10.1016/j.ijmst.2018.08.012.

Tan, Y. L., Zhang, L. J. and Yang, H. M. 2008. On the stress distribution at the bonding interface between rock and bolt. *Geomechanics and Geoengineering*, 3(1), 71-77. doi:https://doi.org/10.1080/17486020701757861.

Ward, W., Coats, D. and Tedd, P. 1976. Performance of tunnel support systems in the Four Fathom Mudstone. *Building Research Establishment. Garston, Watford, Current Paper CP 25/76*, (34630), 11.

Ward, W., Tedd, P. and Berry, N. 1983. The Kielder experimental tunnel: final results. *Geotechnique*, 33(3), 275-291. doi:https://doi.org/10.1680/geot.1983.33.3.275.

Zhang, K., *et al.* 2015. Stress evolution in roadway rock bolts during mining in a fully mechanized longwall face, and an evaluation of rock bolt support design. *Rock mechanics and rock engineering*, 48(1), 333-344. doi:https://doi.org/10.1007/s00603-014-0546-4.

Zhu, C., *et al.* 2015. Modeling of grout crack of rockbolt grouted system. *International Journal of Mining Science and Technology*, 25(1), 73-77. doi:https://doi.org/10.1016/j.ijmst.2014.11.005

Table 1. Estimation of GSI^{res} from GSI^{peak} values (Alejano et al. 2010)

GSI^{peak}	GSI^{res}
75	35-45
70	30-40
60	28-37
50	25-33
40	23-30
30	21-27
25	20-25

Table 2. Various parameters used in the parametric study

Parameter	Unit	Symbol	Value
Intact rock constant	-	m_i	10
Unit weight of rock mass	$\frac{kN}{m^3}$	γ_r	26
Poisson's ratio of rock mass	-	ν_r	0.25
Elastic modulus of rockbolt	GPa	E_{rb}	210
Tensile capacity of rockbolt	MN	T_{rb}	0.2
Shear modulus of rockbolt	GPa	G_g	9
Diameter of rockbolt	m	d	0.025
Grout thickness	m	t	0.0175
Uniaxial compression strength of grout	MPa	-	20
Elastic modulus of shotcrete	GPa	E_{shot}	20
Poisson's ratio of shotcrete	-	ν_{shot}	0.15

Table 3. Rock mass and rockbolt properties of Kielder experimental tunnel (Ward et al. 1976 and 1983, Freeman 1978)

Parameter	Unit	Value
Geological Strength Index (GSI) [1]	-	33
Uniaxial compressive strength (σ_{ci})	MPa	37
m	-	0.1
s	-	0.00008
Cohesion (c)	MPa	0.179
Friction angle ($\emptyset$)	(^{0})	31.4
Dilation angle (Ψ) [2]	(^{0})	0
Poisson's ratio of rock mass (ν_r)	-	0.25
Elastic modulus of rock mass (E_r)	GPa	5
Bolt length	m	1.8
Bolt diameter	m	0.025
Hole diameter	m	0.050
Circumferential spacing between bolts (S_c)	m	0.90
Longitudinal spacing between bolts (S_l)	m	0.90
Shotcrete thickness	cm	14
Elastic modulus of shotcrete layer (early age) [3]	GPa	2

[1] GSI = RMR_{76}

[2] Assumed by authors according to Hoek and Brown (1997)

[3] Assumed by Stille et al. (1989)

Table 4. Various classes depending on $\frac{\sigma_{cm}}{P_0}$ value

$\frac{\sigma_{cm}}{P_0}$	More than 0.25	0.10 to 0.25	Up to 0.10
Class	B	B	C

Table 5. The values of the parameters in the parametric study

Test	GSI^{peak}	P_0 (MPa)	σ_{ci} (MPa)	$\frac{\sigma_{cm}}{P_0}$	Class
1	25	13	45.96	0.05	C
2	25	20.8	73.54	0.05	C
3	25	5.2	18.38	0.05	C
4	40	20.8	28.84	0.05	C
5	25	5.2	51.48	0.14	B
6	40	13	50.48	0.14	B
7	50	20.8	46.63	0.14	B
8	25	5.2	73.54	0.20	B
9	40	13	72.11	0.20	B
10	60	20.8	38.46	0.20	B
11	40	5.2	40.38	0.28	A
12	50	13	58.29	0.28	A
13	60	20.8	53.84	0.28	A
14	40	5.2	63.46	0.44	A
15	60	13	52.88	0.44	A
16	75	20.8	36.70	0.44	A

Table 6. The results of the tunnel supported by only fully grouted rockbolts (S_l = 1 m). Key: ε_m, the unsupported tunnel strain; ε_b, the tunnel strain in the bolt head; ε_m the tunnel strain in the middle between two rockbolts; ε_{mbf}, the tunnel strain in the middle of four rockbolts

Test	Cases	$\frac{\sigma_{cm}}{P_0}$	ε_b (%)	ε_m (%)	ε_{un} (%)	$\frac{\varepsilon_b}{\varepsilon_{un}}$ (%)	$\frac{\varepsilon_m}{\varepsilon_{un}}$ (%)	$\frac{\varepsilon_{mbf}}{\varepsilon_{un}}$ (%)
1	GSI = 25, P_0 = 13 MPa, σ_{ci} = 45.96 MPa	0.05	5.020	5.127	5.651	88.82	90.73	90.87
2	GSI = 25, P_0 = 20.8 MPa, σ_{ci} = 73.54 MPa	0.05	8.293	8.449	9.041	91.72	93.45	93.54
3	GSI = 40, P_0 = 20.8 MPa, σ_{ci} = 28.84 MPa	0.05	3.318	3.374	3.688	89.97	91.49	91.56
4	GSI = 25, P_0 = 5.2 MPa, σ_{ci} = 18.38 MPa	0.05	1.779	1.833	2.260	78.70	81.10	81.38
5	GSI = 25, P_0 = 5.2 MPa, σ_{ci} = 51.48 MPa	0.14	0.925	0.951	1.051	87.92	90.45	90.60
6	GSI = 40, P_0 = 13 MPa, σ_{ci} = 50.48 MPa	0.14	0.843	0.856	0.916	91.98	93.45	93.55
7	GSI = 50, P_0 = 20.8 MPa, σ_{ci} = 46.63 MPa	0.14	0.839	0.849	0.925	90.76	91.79	92.08
8	GSI = 25, P_0 = 5.2 MPa, σ_{ci} = 73.54 MPa	0.20	0.774	0.795	0.877	88.18	90.58	90.72
9	GSI = 40, P_0 = 13 MPa, σ_{ci} = 72.11 MPa	0.20	0.687	0.698	0.734	93.55	95.06	95.15
10	GSI = 60, P_0 = 20.8 MPa, σ_{ci} = 38.46 MPa	0.20	0.448	0.463	0.491	91.29	94.21	94.36
11	GSI = 40, P_0 = 5.2 MPa, σ_{ci} = 40.38 MPa	0.28	0.215	0.220	0.250	86.01	87.83	87.97
12	GSI = 50, P_0 = 13 MPa, σ_{ci} = 58.29 MPa	0.28	0.323	0.327	0.341	94.54	95.70	95.77
13	GSI = 60, P_0 = 20.8 MPa, σ_{ci} = 53.84 MPa	0.28	0.327	0.335	0.365	89.70	91.88	91.94
14	GSI = 40, P_0 = 5.2 MPa, σ_{ci} = 63.46 MPa	0.44	0.194	0.198	0.212	91.56	93.07	93.15
15	GSI = 60, P_0 = 13 MPa, σ_{ci} = 52.88 MPa	0.44	0.154	0.156	0.161	95.65	96.48	96.56
16	GSI = 75, P_0 = 20.8 MPa, σ_{ci} = 36.70 MPa	0.44	0.142	0.147	0.159	89.23	92.71	93.03

Table 7. The influence radius of a bolt in the various conditions

Test	Cases	The influence radius of a bolt (R) (m)
1	GSI = 25, P_0 = 13 MPa, σ_{ci} = 45.96 MPa	0.75
2	GSI = 25, P_0 = 20.8 MPa, σ_{ci} = 73.54 MPa	0.6
3	GSI = 40, P_0 = 20.8 MPa, σ_{ci} = 28.84 MPa	0.75
4	GSI = 25, P_0 = 5.2 MPa, σ_{ci} = 18.38 MPa	1
5	GSI = 25, P_0 = 5.2 MPa, σ_{ci} = 51.48 MPa	0.75
6	GSI = 40, P_0 = 13 MPa, σ_{ci} = 50.48 MPa	0.6
7	GSI = 50, P_0 = 20.8 MPa, σ_{ci} = 46.63 MPa	0.75
8	GSI = 25, P_0 = 5.2 MPa, σ_{ci} = 73.54 MPa	1
9	GSI = 40, P_0 = 13 MPa, σ_{ci} = 72.11 MPa	0.6
10	GSI = 60, P_0 = 20.8 MPa, σ_{ci} = 38.46 MPa	0.6
11	GSI = 40, P_0 = 5.2 MPa, σ_{ci} = 40.38 MPa	1
12	GSI = 50, P_0 = 13 MPa, σ_{ci} = 58.29 MPa	0.6
13	GSI = 60, P_0 = 20.8 MPa, σ_{ci} = 53.84 MPa	0.75
14	GSI = 40, P_0 = 5.2 MPa, σ_{ci} = 63.46 MPa	0.6
15	GSI = 60, P_0 = 13 MPa, σ_{ci} = 52.88 MPa	0.5
16	GSI = 75, P_0 = 20.8 MPa, σ_{ci} = 36.70 MPa	0.75

Table 8. The results of the tunnel supported by fully grouted rockbolts and the shotcrete layer. Key: ε_m, the unsupported tunnel strain; S_l, longitudinal spacing between bolts

Cases	ε_b (%) (S_l =1 m, t = 0.2 m)	ε_m (%) (S_l =1 m, t = 0.2 m)	ε_b (%) (S_l =1.5 m, t = 0.25 m)	ε_m (%) (S_l =1.5 m, t = 0.25 m)	ε_b (%) (S_l =2 m, t = 0.3 m)	ε_m (%) (S_l =2 m, t = 0.3 m)
GSI = 25, P_0 = 13 MPa, σ_{ci} = 45.96 MPa	2.3389	2.3704	2.3947	2.5167	2.4864	2.7548
GSI = 25, P_0 = 20.8 MPa, σ_{ci} = 73.54 MPa	1.0251	1.0381	1.0299	1.0693	1.0587	1.1292
GSI = 40, P_0 = 20.8 MPa, σ_{ci} = 28.84 MPa	0.4412	0.4536	0.4456	0.4666	0.4466	0.4822
GSI = 25, P_0 = 5.2 MPa, σ_{ci} = 51.48 MPa	1.4566	1.4766	1.4964	1.5728	1.5573	1.7247
GSI = 40, P_0 = 13 MPa, σ_{ci} = 50.48 MPa	0.4330	0.4405	0.4351	0.4506	0.4273	0.4536
GSI = 50, P_0 = 20.8 MPa, σ_{ci} = 46.63 MPa	0.4260	0.4270	0.4174	0.4281	0.4170	0.4369
GSI = 25, P_0 = 5.2 MPa, σ_{ci} = 73.54 MPa	0.4291	0.4407	0.4286	0.4467	0.4276	0.4565
GSI = 40, P_0 = 13 MPa, σ_{ci} = 72.11 MPa	0.3991	0.4057	0.3984	0.4089	0.3878	0.4028
GSI = 60, P_0 = 20.8 MPa, σ_{ci} = 38.46 MPa	0.2667	0.2677	0.2593	0.2680	0.2501	0.2642
GSI = 40, P_0 = 5.2 MPa, σ_{ci} = 40.38 MPa	0.1465	0.1488	0.1452	0.1488	0.1435	0.1480
GSI = 50, P_0 = 13 MPa, σ_{ci} = 58.29 MPa	0.2072	0.2093	0.2042	0.2077	0.1998	0.2043
GSI = 60, P_0 = 20.8 MPa, σ_{ci} = 53.84 MPa	0.2257	0.2269	0.2252	0.1397	0.2124	0.2227
GSI = 40, P_0 = 5.2 MPa, σ_{ci} = 63.46 MPa	0.1410	0.1427	0.1397	0.1420	0.1386	0.1415
GSI = 60, P_0 = 13 MPa, σ_{ci} = 52.88 MPa	0.1112	0.1119	0.1101	0.1115	0.1083	0.1096
GSI = 75, P_0 = 20.8 MPa, σ_{ci} = 36.70 MPa	0.1090	0.1100	0.1058	0.1095	0.1012	0.1090

Figures Captions:

Figure 1. Perspective view of the numerical model

Figure 2. Schematic 2D view of the problem

Figure 3. The geometry of the model after installing the rockbolts

Figure 4. 3D view of the systematic rockbolt reinforcement around the tunnel

Figure 5. Comparison of the increase of the radial stress in the tunnel wall due to the bolting effect by the numerical and the analytical methods

Figure 6. Schematic view of the tunnel surface displacements

Figure 7. Tunnel surface displacements between two adjacent bolts (S_l = S_c = 1 m, GSI = 25, P_0 = 13 MPa, σ_{ci} = 45.96 MPa)

Figure 8. The tunnel convergence between the bolts in the longitudinal direction vs bolts spacing for unsupported and supported tunnels in a) Class A b) Class B c) Class C (the related unsupported tunnel strain of each test is shown by a dash line with the same colour)

Figure 9. The reference points to record the maximum displacements (A: middle of two bolts in the circumferential direction, B: middle of two bolts in the longitudinal direction, C: middle of four bolts)

Figure 10. $\frac{\sigma_{cm}}{P_0}$ vs ε_m (%) for unsupported and supported tunnels with fully grouted rockbolts and the shotcrete layer. Key: S_l, longitudinal spacing between bolts; t, shotcrete layer thickness

Figure 11. The average maximum bending moment for different rock masses. Key: S_l, longitudinal spacing between bolts; t, shotcrete layer thickness

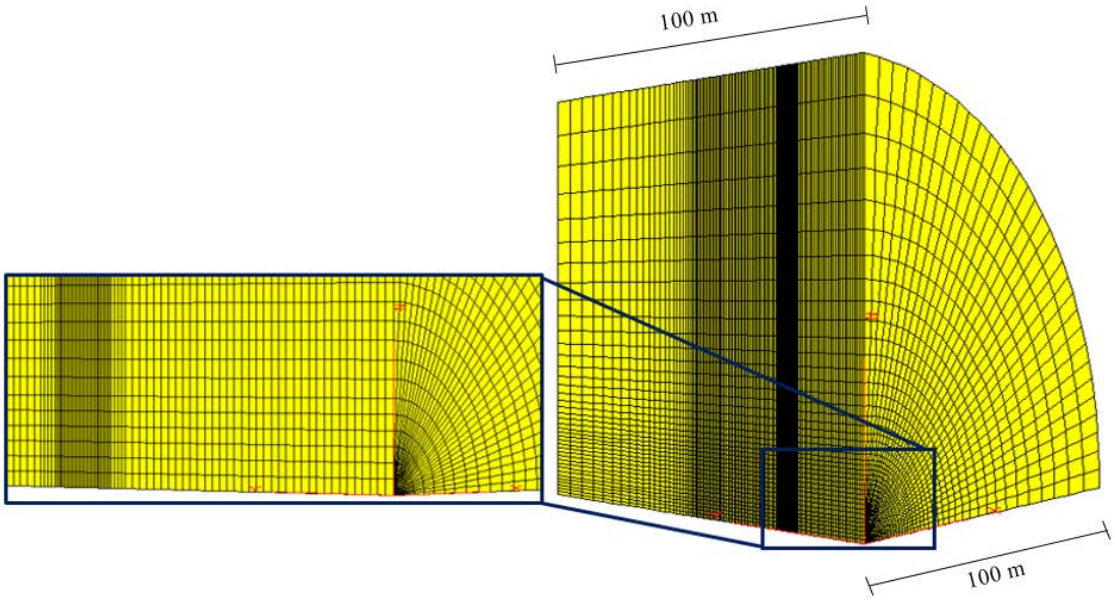

Figure 1. Perspective view of the numerical model

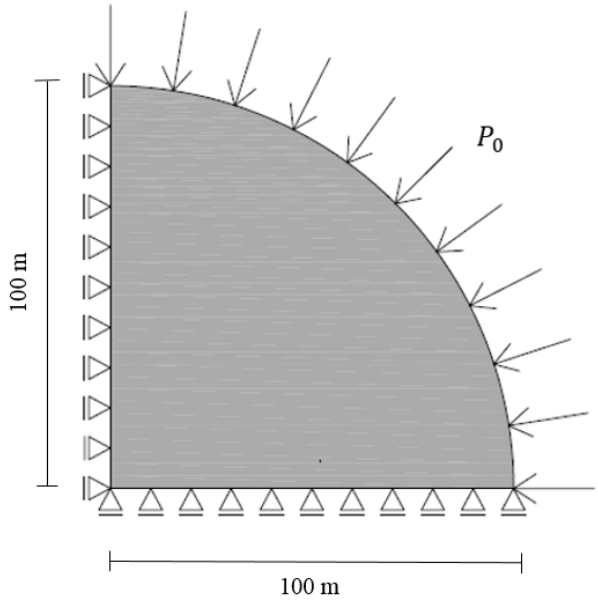

Figure 2. Schematic 2D view of the problem

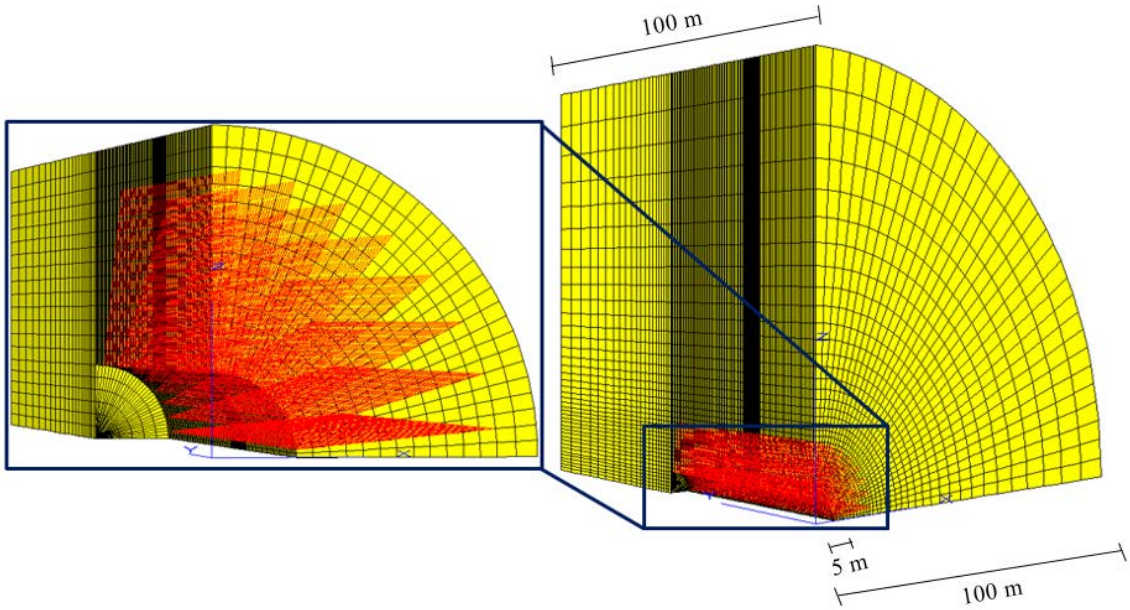

Figure 3. The geometry of the model after installing the rockbolts

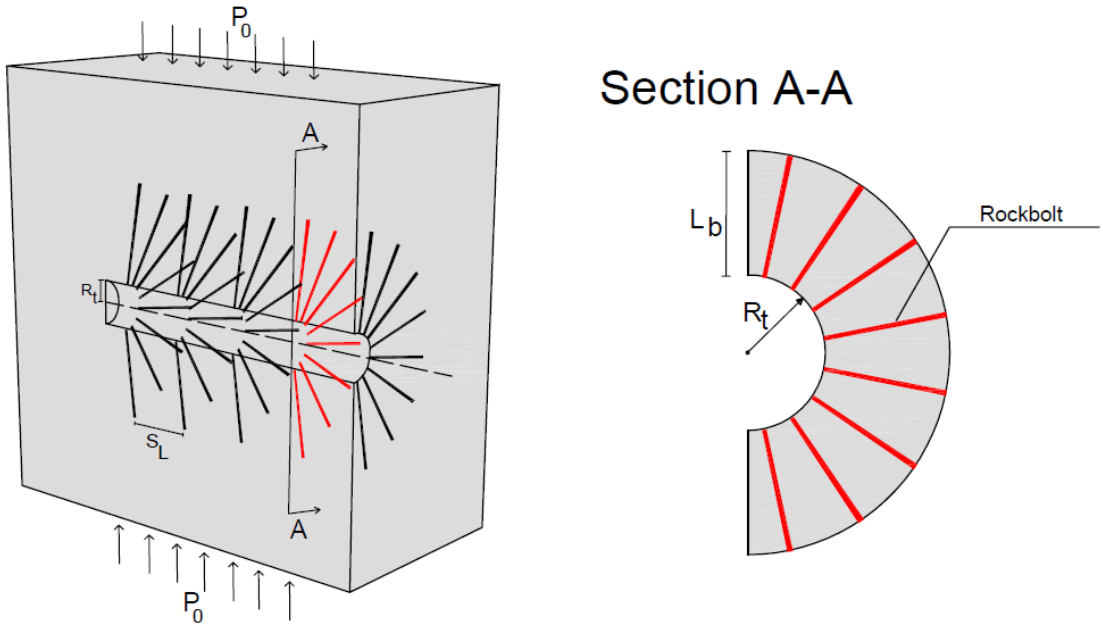

Figure 4. 3D view of the systematic rockbolt reinforcement around the tunnel

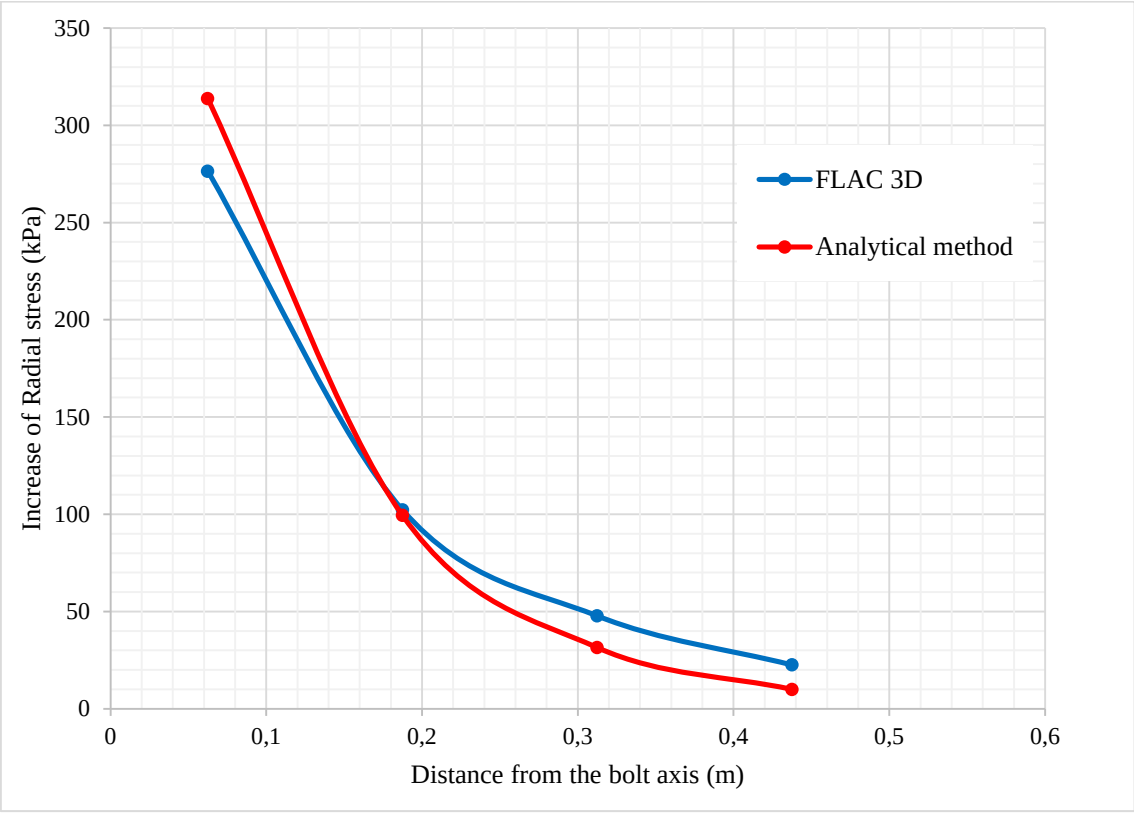

Figure 5. Comparison of the increase of the radial stress in the tunnel wall due to the bolting effect by the numerical and the analytical methods

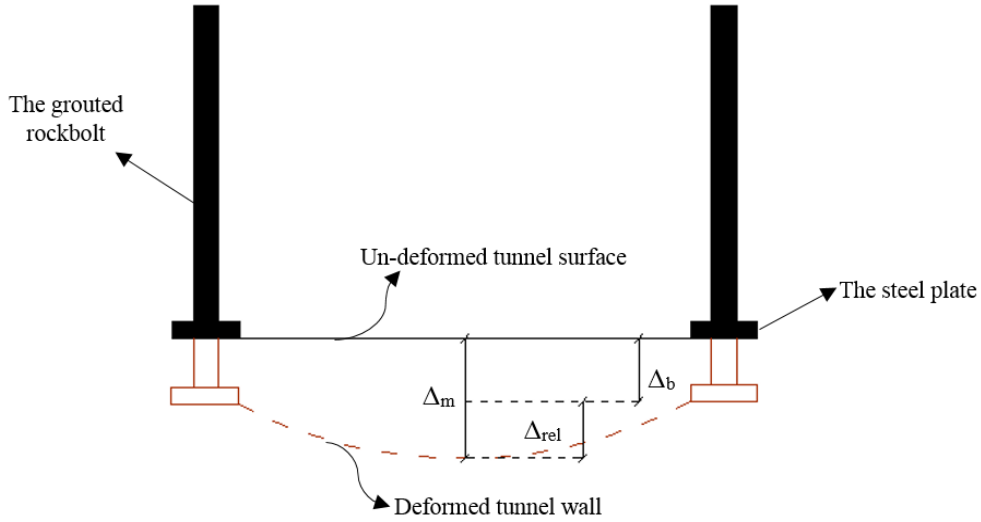

Figure 6. Schematic view of the tunnel surface displacements

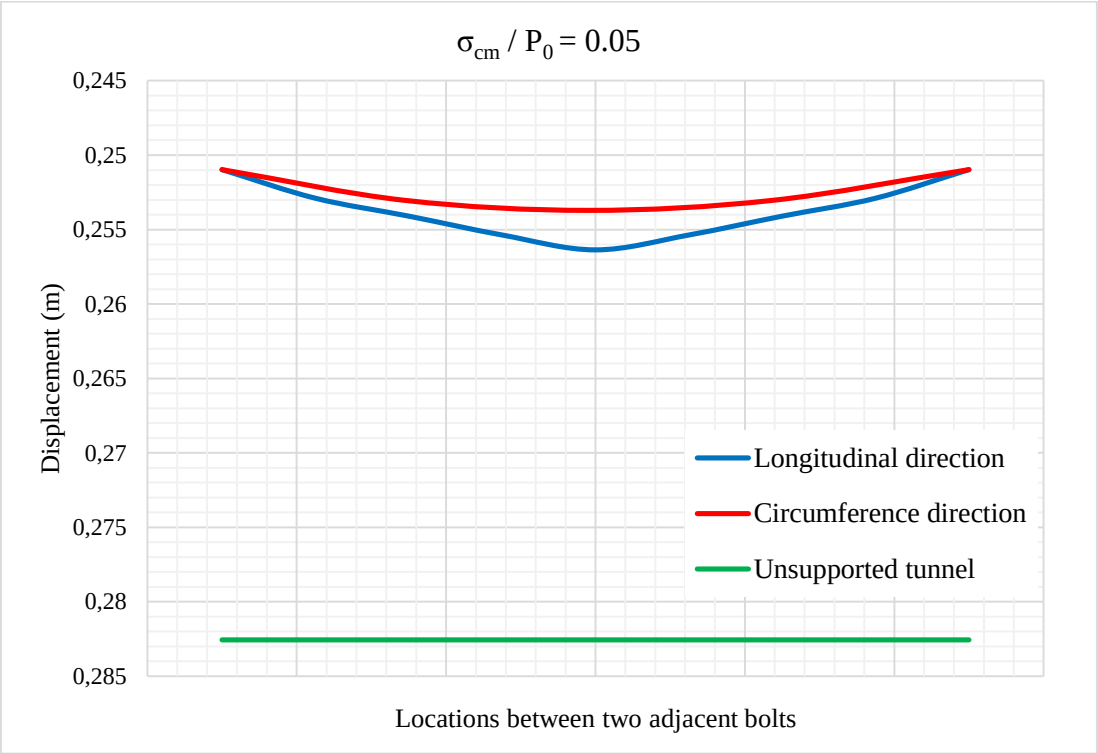

Figure 7. Tunnel surface displacements between two adjacent bolts (S_l = S_c = 1 m, GSI = 25, P_0 = 13 MPa, σ_{ci} = 45.96 MPa)

a)

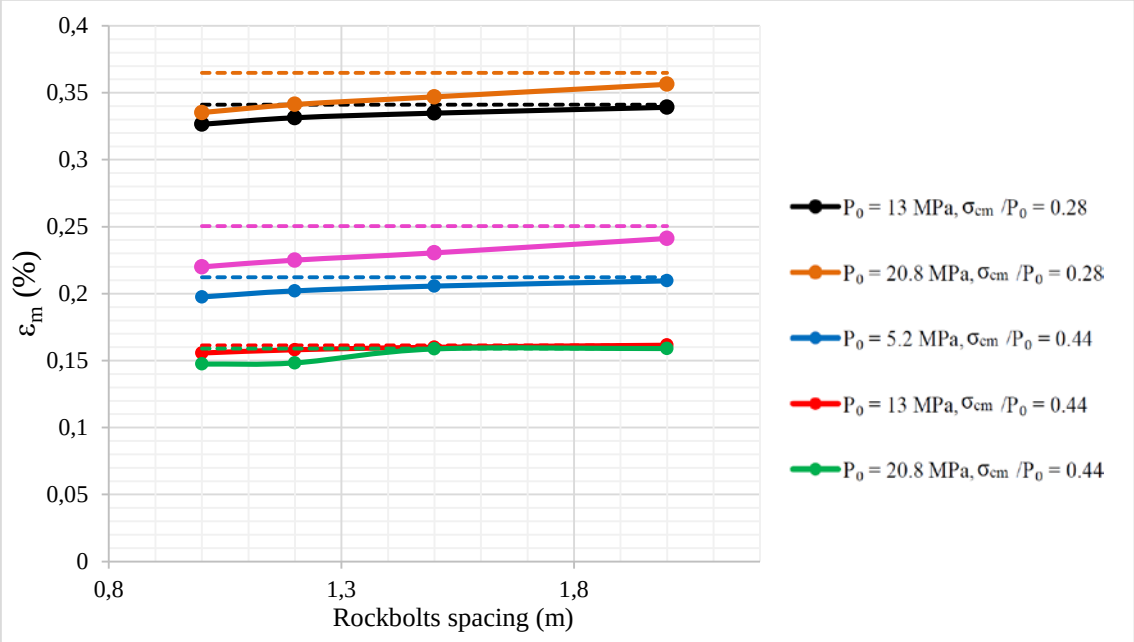
0,4
0,35
0,3
0,25
0,2
0,15
0,1
0,05
0
ε_m (%)
0,8
1,3
1,8
Rockbolts spacing (m)
P_0 = 13 MPa, σ_{cm} /P_0 = 0.28
P_0 = 20.8 MPa, σ_{cm} /P_0 = 0.28
P_0 = 5.2 MPa, σ_{cm} /P_0 = 0.44
P_0 = 13 MPa, σ_{cm} /P_0 = 0.44
P_0 = 20.8 MPa, σ_{cm} /P_0 = 0.44

b)

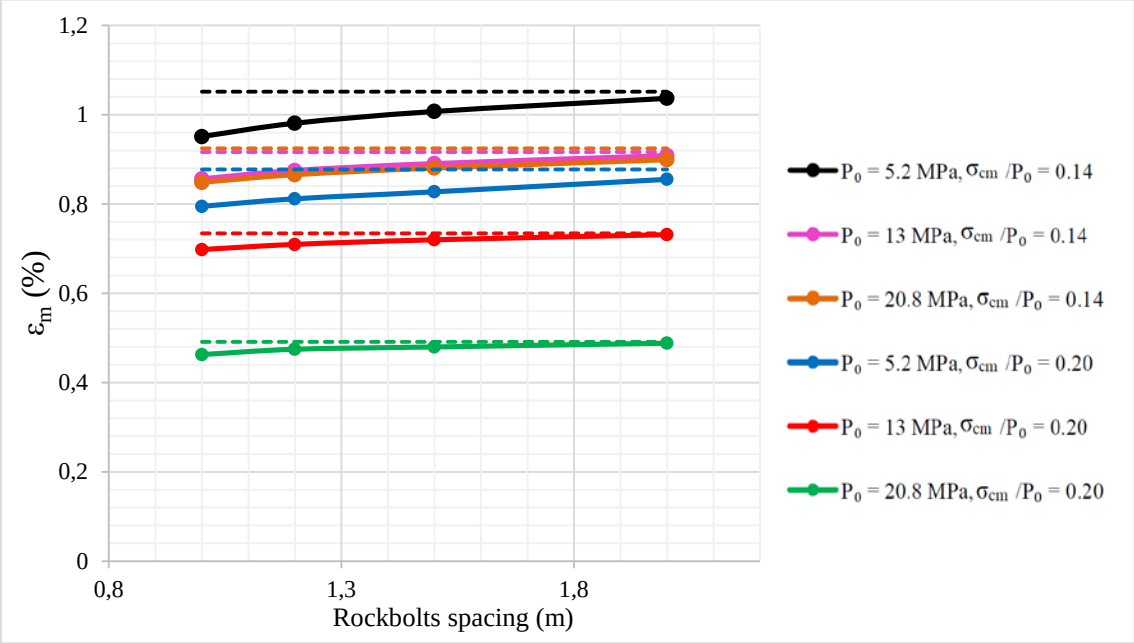
1,2
1
0,8
0,6
0,4
0,2
0
ε_m (%)
0,8
1,3
1,8
Rockbolts spacing (m)
P_0 = 5.2 MPa, σ_{cm} /P_0 = 0.14
P_0 = 13 MPa, σ_{cm} /P_0 = 0.14
P_0 = 20.8 MPa, σ_{cm} /P_0 = 0.14
P_0 = 5.2 MPa, σ_{cm} /P_0 = 0.20
P_0 = 13 MPa, σ_{cm} /P_0 = 0.20
P_0 = 20.8 MPa, σ_{cm} /P_0 = 0.20

c)

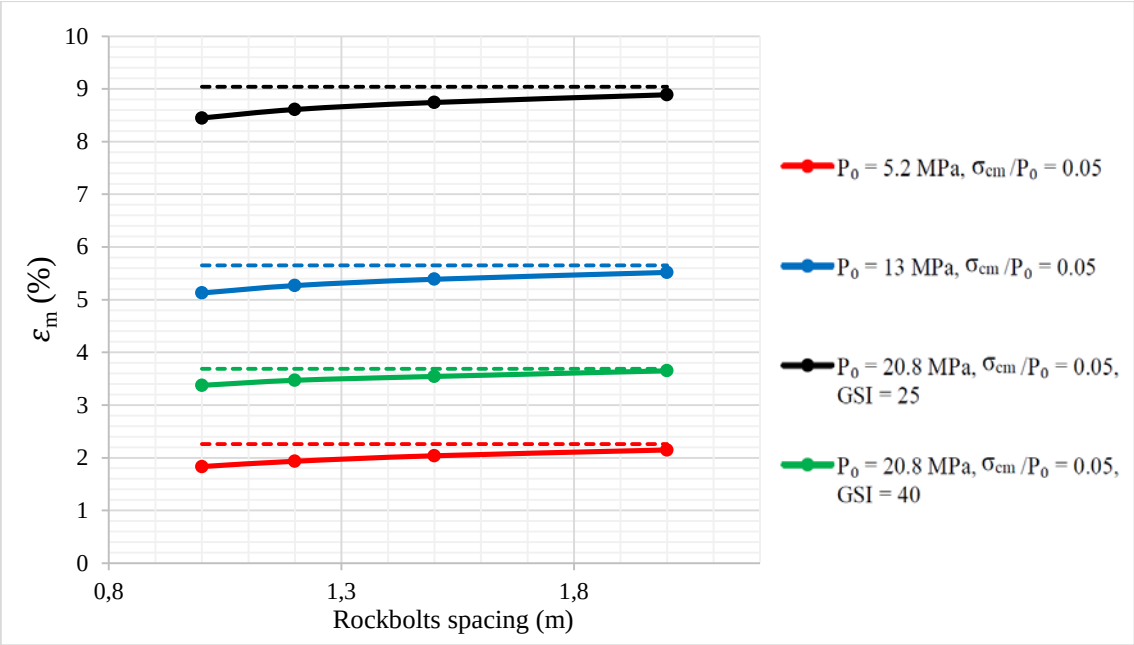

Figure 8. The tunnel convergence between the bolts in the longitudinal direction vs bolts spacing for unsupported and supported tunnels in a) Class A b) Class B c) Class C (the related unsupported tunnel strain of each test is shown by a dash line with the same colour)

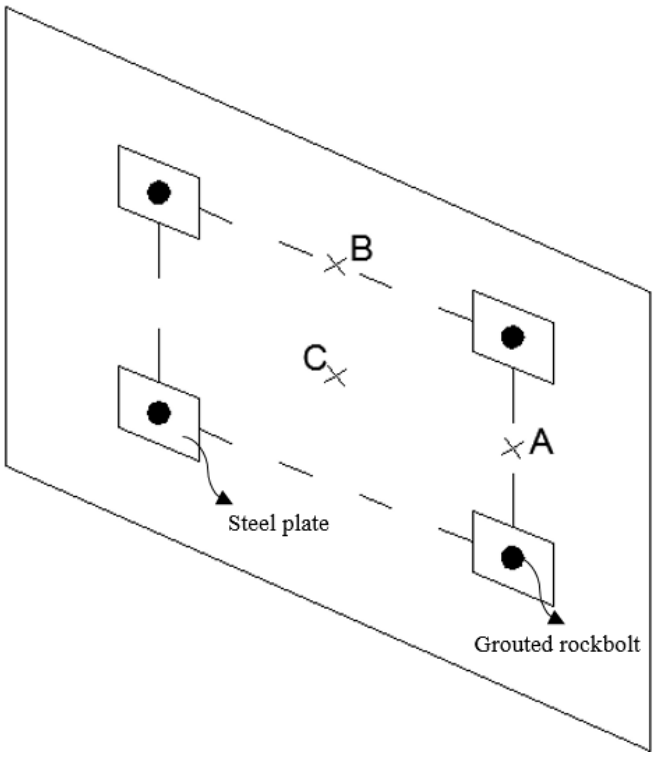

Figure 9. The reference points to record the maximum displacements (A: middle of two bolts in the circumferential direction, B: middle of two bolts in the longitudinal direction, C: middle of four bolts)

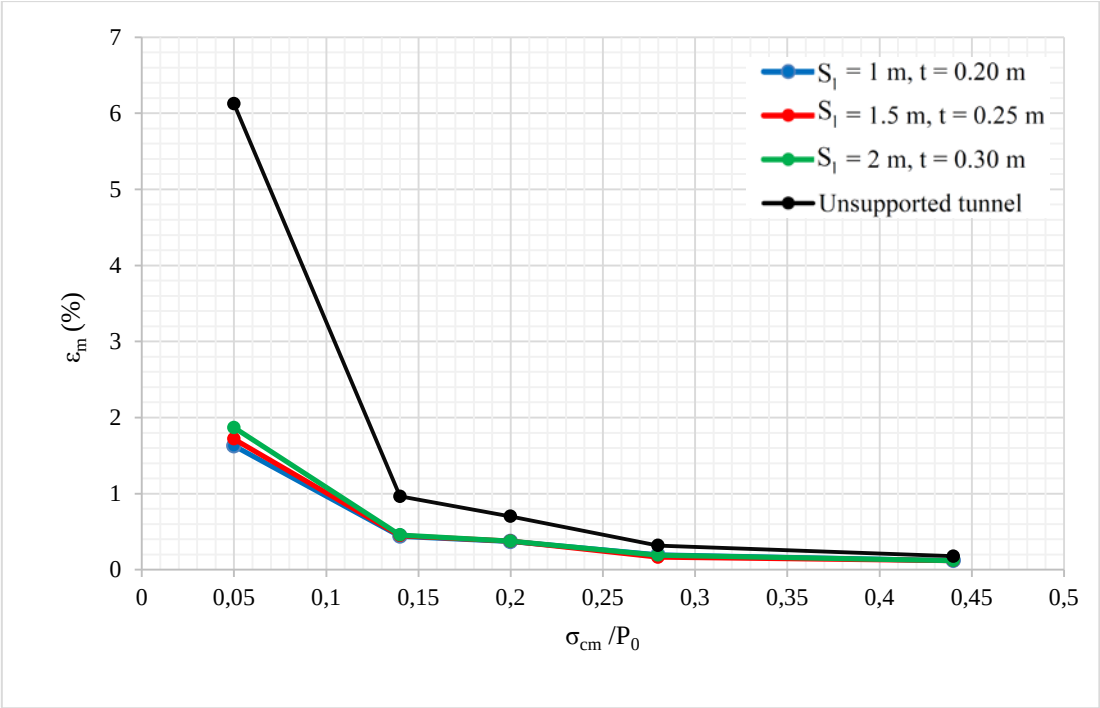

Figure 10. $\frac{\sigma_{cm}}{P_0}$ vs ε_m (%) for unsupported and supported tunnels with fully grouted rockbolts and the shotcrete layer. Key: S_l, longitudinal spacing between bolts; t, shotcrete layer thickness

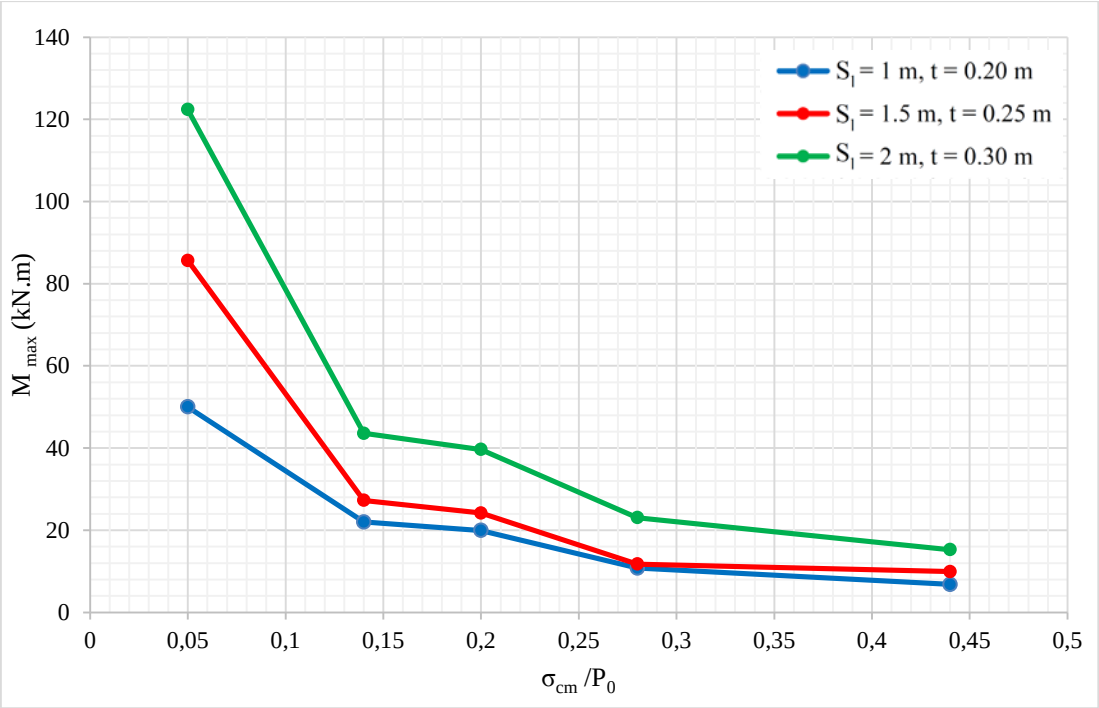

Figure 11. The average maximum bending moment for different rock masses. Key: S_l, longitudinal spacing between bolts; t, shotcrete layer thickness